

# Antiparticle to Particle Production Ratios in hadron–hadron and d–Au collisions in the DPMJET-III Monte Carlo

F. W. Bopp\* and J. Ranft†  
*Fachbereich Physik, Universität Siegen, D-57068 Siegen, Germany*

R. Engel‡  
*Forschungszentrum Karlsruhe, Institut für Kernphysik, Postfach 3640, D-76021 Karlsruhe*

S. Roesler§  
*CERN, Geneva, Switzerland*

To understand baryon stopping we analyse new RHIC and Fermilab data within the framework of the multichain Monte Carlo DPMJET-III. The present consideration is restricted to hadron–hadron and d–Au collisions.

## I. INTRODUCTION

The theoretical tools available at present are not sufficient to understand hadronic collisions at high energies from QCD alone. Phenomenological models of so-called *soft* multiparticle production are typically applied in addition to perturbative QCD. The Dual Parton Model (DPM) [1] is such a phenomenological model. It is quite successful in its understanding of many details in the multiparticle production. Its fundamental ideas are presently the basis of many of the Monte Carlo implementations of soft interactions.

The properties of our DPM implementation DPMJET-III are described in [2, 3, 4, 5, 6]. For a more detailed description of DPMJET-III we refer to these papers and the literature quoted therein.

A feature of hadron production in nuclear collisions discussed in the last 10 years is the large stopping of the participating nucleons in hadron–nucleus and nucleus–nucleus collisions. Experimental data clearly demonstrating the sizable stopping of the participating nucleons in hadron–nucleus and nucleus–nucleus interactions for fixed-target experiments have been presented in [7, 8, 9] and [10].

Multistring fragmentation models like the Dual Parton Model (DPM) or similar models contain some stopping, but in their original form they did not account for the enhanced stopping found in nuclear collisions. Therefore, in order to incorporate the effect into multistring fragmentation models new diquark breaking DPM–diagrams acting in hadron–nucleus and nucleus–nucleus collisions were proposed by [11] and [12] and investigated in detail in [13] and [14]. Similar ideas were discussed by [15] and [16]. The Monte Carlo implementation into DPMJET-II.5 of the new diquark breaking diagrams of

[11] and [12] was discussed in [17]. The implementation into DPMJET-III [6] of these diagrams differs somewhat from that of [17] and was described in [18, 19].

A second mechanism, which can contribute to baryon stopping in nuclear collisions occurs during the fusion of chains [20, 21]. This mechanism was introduced into DPMJET-III in order to accommodate the RHIC data [22, 23]. We will use chain fusion here exactly as described in these papers.

Particle production ratios in p–p and d–Au collisions measured at RHIC [24, 25, 26, 28] allow us a more precise determination of the parameters of anomalous baryon stopping. Needed stopping contribution are described in section II. Sections III and IV consider the available data on stopping for proton–proton, deuteron–gold reactions. In section V we consider hyperon productions ratios in pion–proton collisions. There we need another new mechanism to describe the data.

## II. IMPLEMENTATION OF NEW DIAGRAMS FOR AN IMPROVED DESCRIPTION OF BARYON STOPPING

As justified by Rossi and Veneziano [29] in the framework of a  $1/N$  expansion a baryon can be pictured as made out of three quarks bound together by three strings which join in a so-called string junction point. In diagrams one can characterize the baryons

- (i) by the three quarks and the string junction or
- (ii) by a quark and a diquark.

In the second case the string junction always goes with the diquark.

Figs. 1-4 are quark line diagrams describing the production chains of particles. In these diagrams quarks and diquarks are usually plotted as single resp. paired solid lines. If diquarks break, string junctions are added as dashed lines.

In the fragmentation of diquarks there are two possibilities for the first fragmentation step. Either one gets a baryon, which contains the diquark (with the string junction) in the first step or one gets a meson containing only

\*Electronic address: bopp@physik.uni-siegen.de

†Electronic address: Johannes.Ranft@cern.ch

‡Electronic address: Ralph.Engel@ik.fzk.de

§Electronic address: Stefan.Roesler@cern.ch

## A. Nuclear diquark breaking

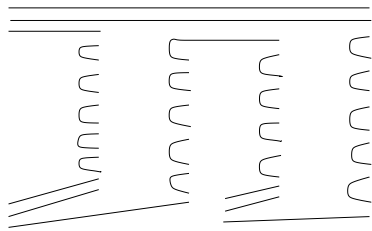


Figure 1: The diquark-conserving diagram for a nucleon-nucleus collision with two participants of the target nucleus.

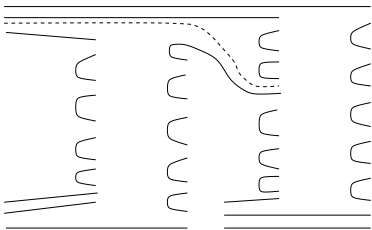


Figure 2: The Glauber sea quark mechanism of baryon stopping GSQBS for a nucleon-nucleus collision with two participants of the target nucleus. This is the second C-K diquark-breaking mechanism [12].

one of the two quarks. In this case the string junction migrates to the next step and the baryon is eventually produced in one of the following fragmentation steps.

This mechanism is well-known, it is presented in the review on the Dual Parton Model [1] and it was investigated for instance in [30, 31]. This mechanism was implemented a long time ago (1980) in the BAMJET-fragmentation code [32, 33] used in the early versions of DPMJET. This mechanism is also implemented under the name *popcorn* fragmentation in the Lund chain fragmentation model JETSET [34, 35] which is presently used in DPMJET.

What happens in the model with the popcorn mechanism compared to the model without can be most easily seen by looking at the proton rapidity distribution in p-p collisions. The two maxima in the target and projectile fragmentation region of the proton rapidity distribution shift by about half a unit to the center, the peaks become wider and correspondingly the dip in the center is reduced. At the same time the Feynman  $x$  distributions of mesons get a component at larger Feynman  $x$ . The effects in hadron-nucleus and nucleus-nucleus collisions are quite similar. However, the popcorn mechanism alone cannot explain the baryon stopping observed experimentally in hadron-nucleus and nucleus-nucleus collisions [7, 8].

Most interesting for DPMJET is the so-called *second C-K* mechanism [12, 13, 14, 36]. In Fig. 1 we plot first the diquark-conserving diagram for a nucleon-nucleus collisions with two participants of the target nucleus. This is the traditional way for such a collision in the DPM. In Fig. 2 we plot the second C-K diquark-breaking diagram for the same collision. Now the second valence quark from the broken diquark is replaced by a Glauber sea quark from the nucleon projectile. Therefore, we will call the mechanism the Glauber sea quark mechanism of baryon stopping (GSQBS). The probability of such a diquark splitting rises if the considered nucleon is involved in more than two interactions.

A new type of string combination appears in the second interaction, which happened between the second valence quark (the top one) and the junction line. A central assumption is that a sea quark of the initial scattering determines the position of the junction line. One of the valence quarks which its initial momentum connects to the junction line by an upward string. In this way the string pulling the vortex line down is compensated by a string pulling it up.

The GSQBS picture is chosen for simplicity. Formally at the very top three strings and a vortex line are exchanged. In the topological view it is a cut t-channel-quarkless-baryonium-exchange. Usually baryonium exchanges have a rather low intercept and the idea is that in special situations a small quarkless component with a high intercept appears. Taking the position from the sea quark a flat distribution of the vortex line with an intercept of one is implied, with an added bias to larger values as the sea quark actually had to sit on the forward end of string of a minimum size. In the factorizing version of the model[37] this bias does not exist. The intercept is then estimated to be slightly less than one.

The GSQBS has been implemented into DPMJET-II.5 and DPMJET-III. With this mechanism one is able to fill the dip in the baryon rapidity distributions at central rapidity in agreement to the experimental data. As discussed already in detail in [14, 36] this mechanism also contributes to increase the Hyperon production in nucleon-nucleus and nucleus-nucleus collisions.

## B. Hadronic diquark breaking at high energy

At high energies multiple collisions appear even in hadron-hadron scattering due to the unitarization procedure. This has the consequence that new diagrams like the GSQBS diagrams become necessary. In some way or other such diagrams have to be implemented in any model which includes both elastic and inelastic processes.

We call the sea quarks at the ends of the additional chains in this case *unitary sea quarks*. They are relevant for high energies. The Glauber sea quarks are needed in nuclear collisions already at rather low energies, for

instance at the energies of heavy ion collisions at the CERN-SPS. In contrast to this, unitary sea quarks appear in significant numbers only at rather high energies, for instance at the energies of RHIC, the CERN-SPS collider or the Tevatron collider.

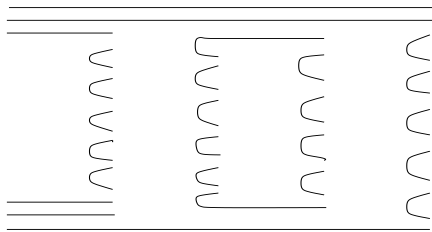


Figure 3: Standard DPM diagram for a nucleon-nucleon interaction with one additional soft secondary interaction induced by the unitarization procedure.

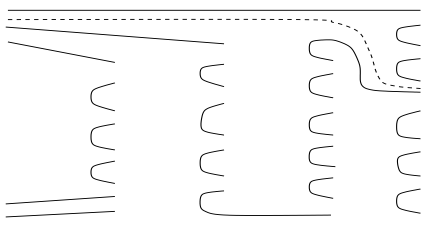


Figure 4: New DPM diagram for a nucleon-nucleon interaction with one additional soft secondary interaction induced by the unitarization procedure. We call this unitary sea quark mechanism for baryon stopping USQBS [17].

With the unitary sea quarks at the ends of the chains from the secondary collisions one obtains a new mechanism for baryon stopping which will become effective at very high energies. It is illustrated in Figs. 3 and 4.

The standard DPM diagram is plotted in Fig. 3 for a nucleon-nucleon interaction with two soft interactions induced by the unitarization procedure. As in Fig. 1, there is one valence-valence and one sea-sea interaction, each represented by a pair of chains. In analogy to Fig. 2, a new diagram [17] for baryon stopping is constructed in Fig. 4. The diquark is split and a unitary sea quark is used to have the baryon only in the second or later fragmentation steps in one of the chains. We call this the unitary sea quark mechanism for baryon stopping USQBS. The implementation of the new diquark breaking diagrams in DPMJET-III is discussed in detail in [18, 19]. The relative probability of this process introduces one parameter, which will be given later.

Again the probability for such a diquark splitting rises if there are more than 2 interactions of the hadrons involved. Obviously, this mechanism leads to Feynman  $x$  distributions of baryons in p-p collisions becoming softer and Feynman  $x$  distributions of mesons becoming harder than without the USQBS mechanism.

In contrast to the GSQBS mechanism which leads already to observable changes in nuclear collisions at the

energy of the CERN-SPS, there were no data available before RHIC to prove that this USQBS mechanism is a needed extension of the DPM. The situation concerning baryon stopping in proton-proton or antiproton-proton collisions at lower energies was inconclusive [38]. An idea to observe baryon stopping in diffractive events [39], which always contain two interactions, was unfortunately not pursued in experimental analysis.

### C. New parameters connected with the diquark breaking diagrams

For each of the new diquark breaking diagrams described in this section a new parameter has to be introduced. These parameters give the probability for the diquark breaking mechanisms to occur, given a suitable sea quark is available and given that the diquark breaking mechanism is kinematically allowed. For an original diquark-quark chain of small invariant mass, which originally just fragments into two hadrons, the diquark breaking is often not allowed at small energies.

The values of the new parameters are determined by comparing DPMJET-III with experimental data on antiparticle to particle production ratios and on net-baryon distributions.

## III. ANTIPARTICLE TO PARTICLE RATIOS IN PROTON-PROTON COLLISIONS

With antibaryon to baryon ratios measured at RHIC one is now for the first time in a position to determine the USQBS parameter with good accuracy. In p-p collisions, the contribution of chain fusion is not very large.

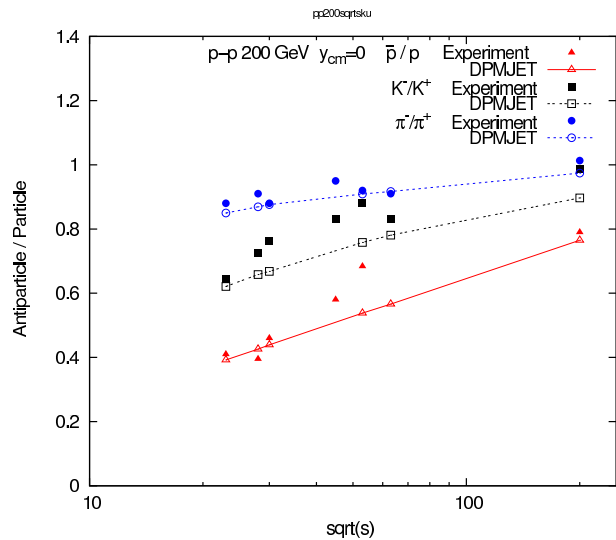


Figure 5:  $\sqrt{s}$  dependence of antiparticle to particle ratios in p-p collisions at  $y_{cm} = 0$ . Experimental data are from the BRAHMS Collaboration at RHIC [28], the ISR [40] and the NA27 Collaboration [41]. We compare DPMJET-III results with the experimental data.

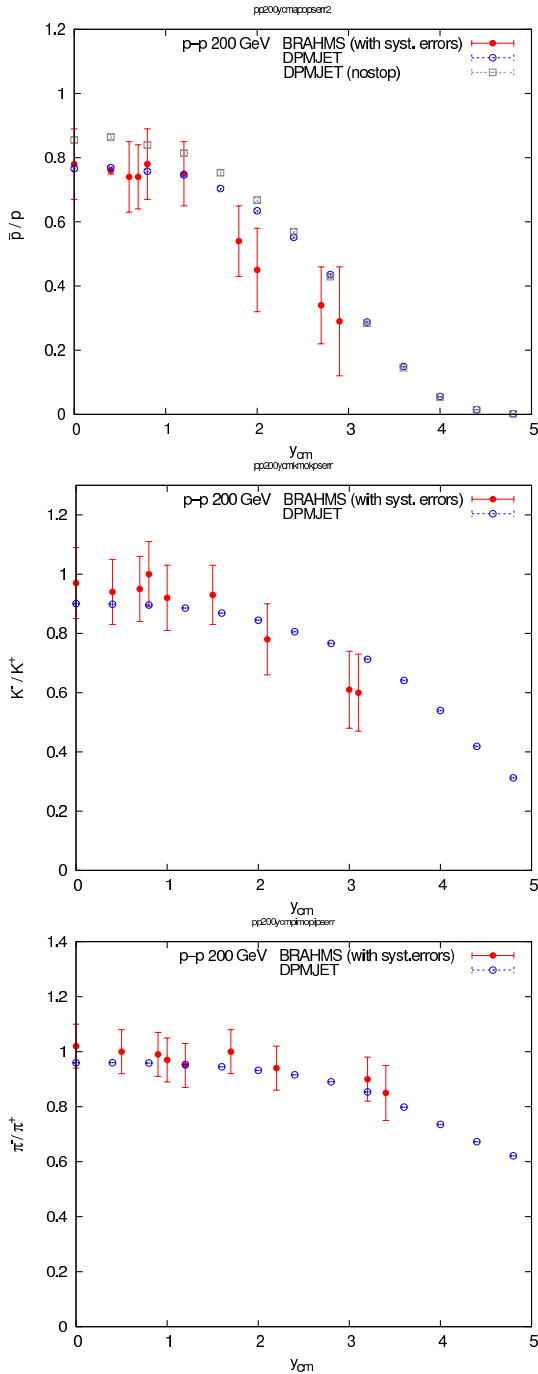


Figure 6: Antiparticle to particle ratios ( $\bar{p}/p$ ,  $K^-/K^+$  and  $\pi^-/\pi^+$ ) in p-p collisions at 200 GeV as function of the cms-rapidity  $y_{cm}$ . We compare data from the BRAHMS Collaboration at RHIC [28] (including the systematic errors as given in the BRAHMS paper) with the results obtained from DPMJET-III. We plot the  $\bar{p}/p$  ratios for the full DPMJET model as well as for the model without the USQBS diagrams ("nostop").

Fig. 5 compares measured  $\pi^-/\pi^+$ ,  $K^-/K^+$  and  $\bar{p}/p$  ratios at  $y_{cm} = 0$  as function of the energy with the DPMJET-III results, of course the USQBS mechanism influences essentially only the antiproton to proton ratio but also the comparison of the antimeson to meson ratios is of interest.

We get agreement to the data for  $\pi^-/\pi^+$  and  $K^-/K^+$ . To obtain agreement with the  $\bar{p}/p$  ratio a USQBS parameter of .07 had to be chosen to get a 0.1 reduction at the highest energy. It means that in 7 % of the possible cases one transforms the diquark conserving diagram as given in Fig. 3 into the diquark breaking diagram given in Fig. 4. It corresponds to the parameter  $\epsilon$  of [37, 42] whose stability against variation in the model was investigated in the cited papers.

The dependence of the three antiparticle to particle production ratios on the cms rapidity of the produced particles is plotted in Fig. 6. Here we have kept the USQBS parameters as determined above in this comparison of DPMJET-III with the BRAHMS data from RHIC [28]. BRAHMS parameters are plotted with statistical and systematic errors as given in [28]. In Fig. 6.a we compare the BRAHMS data for  $\bar{p}/p$  ratios with the full DPMJET model as well as with the model without the USQBS diagrams. It shows that the USQBS diagrams are needed to get a better agreement with the BRAHMS data at central rapidity. In all cases DPMJET-III describes the experimental data practically within the errors.

In Fig.7 we plot the  $p/\pi^+$  particle production ratio as function of the transverse momentum in  $\sqrt{s} = 200$  GeV proton-proton collisions. The particle production ratio according to DPMJET-III is compared with data from the STAR-Collaboration [43]. We find an excellent agreement.

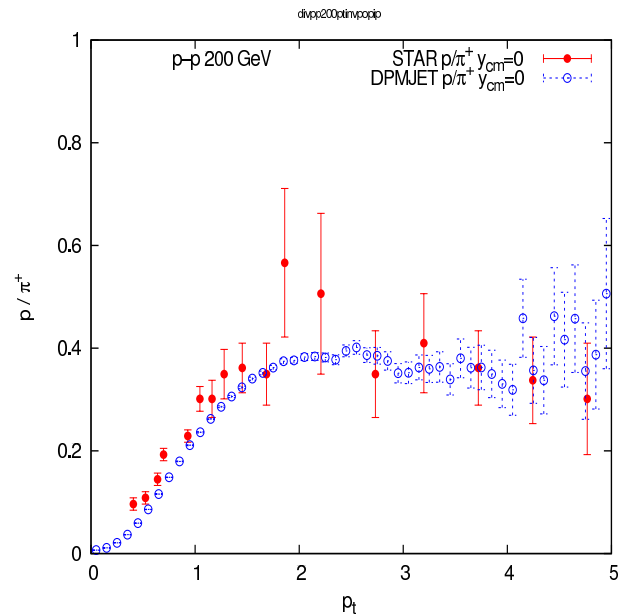


Figure 7: The  $p/\pi^+$  particle production ratio as function of the transverse momentum in  $\sqrt{s} = 200$  GeV proton-proton collisions. We compare the ratio according to DPMJET-III with data from the STAR-Collaboration [43].

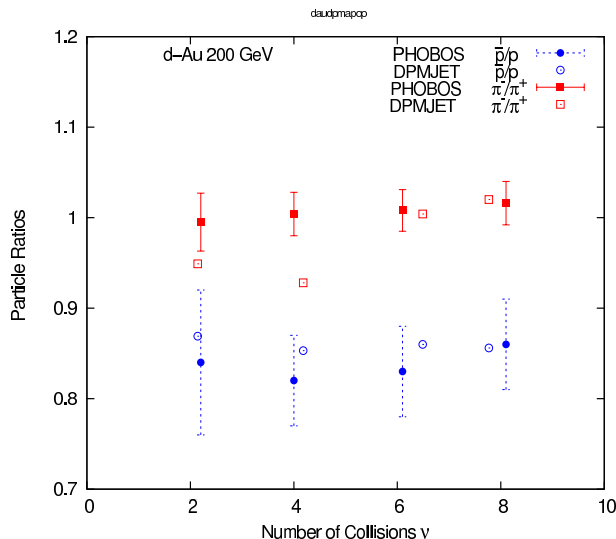


Figure 8: Centrality dependence of charged antiparticle to particle ratios near mid-rapidity as measured by the PHOBOS-Collaboration [25] in d-Au collisions at  $\sqrt{s} = 200$  GeV is compared to the DPMJET-III model.

#### IV. ANTIPARTICLE TO PARTICLE RATIOS IN d – Au COLLISIONS

In d-Au collisions we have, in addition to the baryon stopping mechanisms acting in p-p collisions, also the GSQBS diagrams and the contribution from chain fusion to baryon stopping.

The centrality dependence of charged antiparticle to particle ratios near mid-rapidity was measured by the PHOBOS-Collaboration [24] in d-Au collisions at  $\sqrt{s} = 200$  GeV as function of the centrality. The  $\pi^-/\pi^+$  and  $\bar{p}/p$  ratios are compared in Fig. 8 with the DPMJET-III results. In this comparison the  $\pi^-/\pi^+$  and  $\bar{p}/p$  ratios at all centralities agree within the experimental errors, the statistical errors of the Monte Carlo calculations are below  $\pm 0.02$ .

Regarding the exact position of the points, the measurements and also our DPMJET-III calculations were done for four different centrality bins: 0-10%, 10-30%, 30-60% and 60-100% but the resulting antiparticle to particle ratios are plotted as function of  $\nu$ , the average number of collisions per deuterium participants. PHOBOS finds for the four centralities given above  $\nu = 8.1, 6.1, 4.0$  and  $2.2$ , in the DPMJET-III calculations we find  $\nu = 7.77, 6.49, 4.18$  and  $2.14$ .

In Fig. 9 we plot the  $\bar{p}/p$  and  $\pi^-/\pi^+$  ratios in d-Au collisions at  $\sqrt{s} = 200$  GeV as function of the transverse momentum. Compared are experimental data of the PHOBOS and STAR Collaboration [25, 44] with the results from DPMJET-III, we find a reasonable agreement.

In Figs. 10 and 11 we plot  $\bar{\Lambda}/\Lambda$  ratios and net- $\Lambda$  production ( $\Lambda - \bar{\Lambda}$ ) in d-Au collisions at  $\sqrt{s} = 200$  GeV as

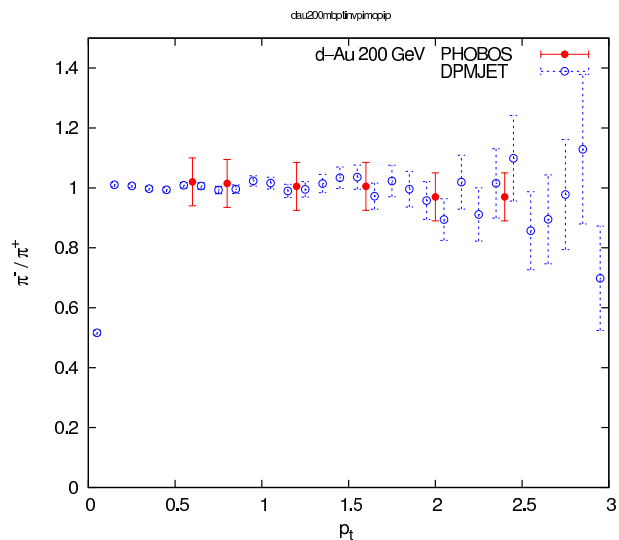
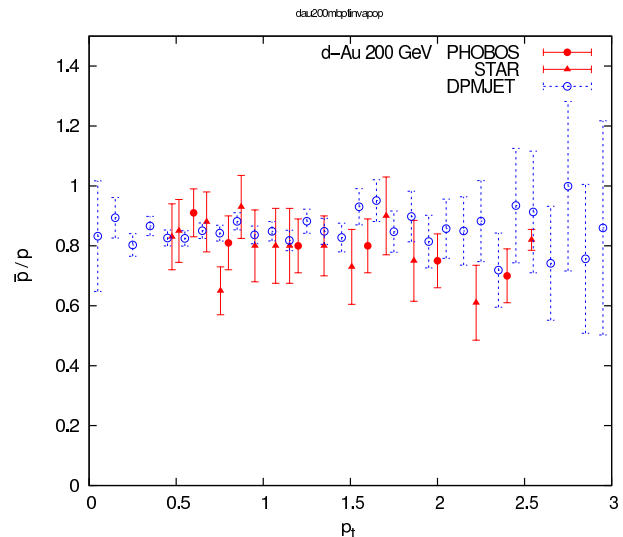


Figure 9: Transverse momentum dependence of the  $\bar{p}/p$  resp.  $\pi^-/\pi^+$  ratio in d-Au collisions at  $\sqrt{s} = 200$  GeV. We compare the data from the PHOBOS and the STAR Collaboration at RHIC [25, 44] to the results from the DPMJET-III model.

function of the cms rapidity. Compared are the experimental data of the STAR Collaboration [26] with the results of the DPMJET-III model. The agreement for the ratios  $\bar{\Lambda}/\Lambda$  is satisfactory given the different binning, significant might be some disagreement for net  $\Lambda$  production in the Au fragmentation region. For all DPMJET-III calculations in Figs. 8 to 11 we use DPMJET-III with chain fusion as described in [22, 23].

The USQBS parameter is used exactly as described in the previous section. The GSQBS parameter is fitted. It turned out to be rather small at this energy and was set to zero in the shown fits.

The vanishing of the GSQBS contribution should not be taken too seriously. In nuclear collision there are two

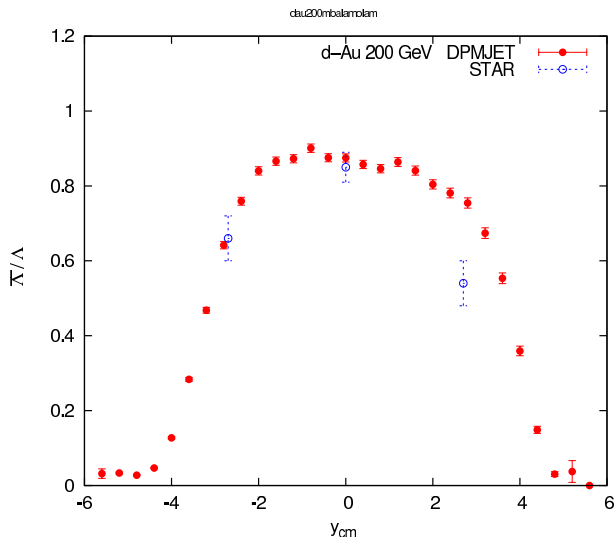


Figure 10: Anti- $\Lambda$  to  $\Lambda$  ratio as function of the cms-rapidity in minimum bias d-Au collisions at  $\sqrt{s} = 200$  GeV. We compare the experimental data from the STAR Collaboration at RHIC [26] to the results from the DPMJET-III model.

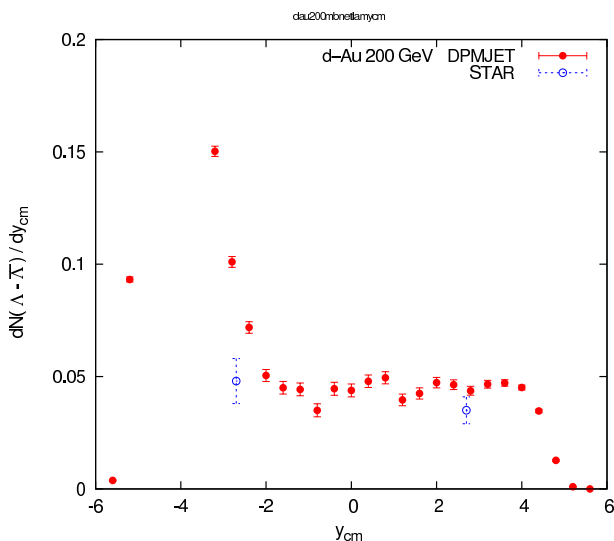


Figure 11: NET- $\Lambda$  production as function of the cms-rapidity in minimum bias d-Au collisions at  $\sqrt{s} = 200$  GeV. We compare the experimental data from the STAR Collaboration at RHIC [26] to the results from the DPMJET-III model.

baryon stopping mechanisms. Besides GSQBS baryon stopping is obtained as a side effect from chain fusion (e.g. a  $qq-q$  chain and a  $\bar{q}-q$  chain can fuse to a  $q-qq$ ) [22, 23]. Both the intricate string structure of GSQBS and the forward-constituents-backward-constituents structure of fusion strings are somewhat ad hoc and an redistribution between both contributions is clearly acceptable. More important is the fact that the observed nuclear baryon stopping is within the expected range (see also [45]).

## V. ANTIHYPERON TO HYPERON RATIOS IN HADRON-HADRON COLLISIONS

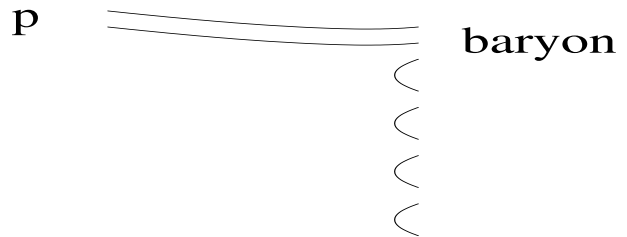


Figure 12: Fragmentation into a baryon, the most important term in the fragmentation of a diquark.

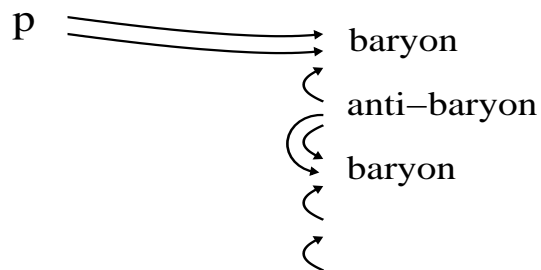


Figure 13: Production of an antibaryon-baryon pair in the standard fragmentation of a diquark.

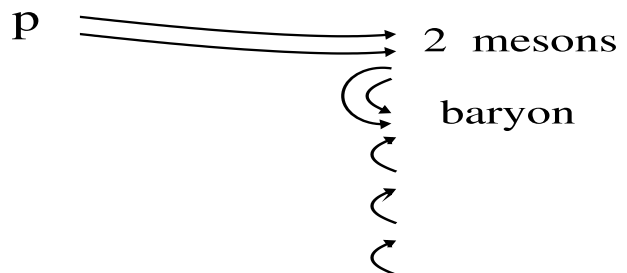


Figure 14: Non-standard fragmentation of a diquark into a leading meson-pair and a baryon.

Asymmetries of strange baryon production in 500 GeV  $\pi^-p$  collisions were measured by the E791 Collaboration at Fermilab [9]. The asymmetry is defined as follows

$$A\left(\frac{B}{\bar{B}}\right) = \frac{N_B - N_{\bar{B}}}{N_B + N_{\bar{B}}} \quad (1)$$

in each  $x_F$  bin. These asymmetries are obviously closely related to the particle production ratios  $\frac{\bar{B}}{B}$ .

All measured asymmetries [9]  $A(\Lambda/\bar{\Lambda})$ ,  $A(\Xi^-/\bar{\Xi}^+)$  and  $A(\Omega^-/\bar{\Omega}^+)$  are positive, correspondingly in the given  $x_F$  range the ratios  $\bar{B}/B$  are smaller than 1, there are more Hyperons produced than anti-Hyperons.

It was already noted by the E791 Collaboration in [9] that the PYTHIA/JETSET code [34, 35] gives  $A(\Omega^-/\bar{\Omega}^+)$  and  $A(\Xi^-/\bar{\Xi}^+)$  asymmetries, which are negative or zero in part of the kinematic range, correspondingly in part of the kinematic range the PYTHIA/JETSET code predicts more double or triple strange anti-Hyperons than Hyperons. This observation was also discussed in detail by Liu et al. [46].

DPMJET-III uses PYTHIA/JETSET for the fragmentation of the hadronic strings, the building blocks of the model. Therefore, we are not surprised that also the original DPMJET-III gives  $A(\Omega^-/\bar{\Omega}^+)$  and  $A(\Xi^-/\bar{\Xi}^+)$  asymmetries, which are negative or zero in part of the kinematic range in contrast to the experimental data.

To find the reason for this wrong behaviour of chain fragmentation models like DPMJET-III or PYTHIA we have to consider the mechanism for baryon (and especially double and triple strange hyperon) production in chain decay models.

In Fig.12 we plot the standard diagram of chain decay models for the fragmentation of a diquark into a leading baryon. In collisions of non-strange hadrons the chain-end diquarks do not contain strange quarks, therefore only hyperons with one strange quark can be produced this way. These are the  $\Lambda$  hyperons in the E791 experiment.

Next, in Fig.13 we plot the diagram for the fragmentation of our chain into a nonleading antibaryon-baryon pair. The antibaryon and baryon do not contain any quarks from the original hadrons involved in the collision. Therefore, each of the quark or antiquarks involved can be strange, the antibaryon and the baryon can be double-strange or even triple-strange hyperons, for instance  $\bar{\Xi}$ ,  $\Xi$ ,  $\bar{\Omega}$  or  $\Omega$  hyperons. But we note according to this mechanism the fragmentation into double-strange or triple-strange anti-hyperons is favored against the fragmentation into double-strange or triple-strange hyperons. This diagram (or slight variations of it) is the only diagram available in the PYTHIA/JETSET chain fragmentation to produce antihyperon-hyperon pairs in diquark fragmentation. This explains the wong behaviour of PYTHIA and DPMJET-III discussed above.

In order to correct the behaviour of DPMJET-III we have to add one missing diagram in diquark fragmentation. We did not correct[47] PYTHIA, but we added the missing fragmentation step in DPMJET-III before calling PYTHIA.

The missing diagram: We note, in the PYTHIA chain fragmentation diquark-antidiquark pairs can be exchanged in any position (see Fig.13) except near to the chain-end diquarks. In Fig.14 we plot the missing diagram. At the chain-end we obtain a diquark-antidiquark pair, this has to fragment into a pair of mesons. Next to this in the chain we obtain a baryon. All three quarks of his baryon can be strange quarks. Therefore, in this diagram we can obtain double-strange and triple-strange hyperons, which dominate against the anti-hyperons produced eventually later in the chain fragmentation. Obvi-

ously, this is the missing mechanism needed in DPMJET-III.

In order to introduce the mechanism according to Fig.14 we have to introduce a new parameter, which describes the probability, that the new diagram is to be used in the first diquark fragmentation step. We obtain good results with the rather small probability of such a baryonium  $B_{2Mesons} = 0.01$ . For the flavor distribution of this baryonium and the exchanged diquark-antidiquark pair we use a rather small value of  $r_s = 5\%$ .

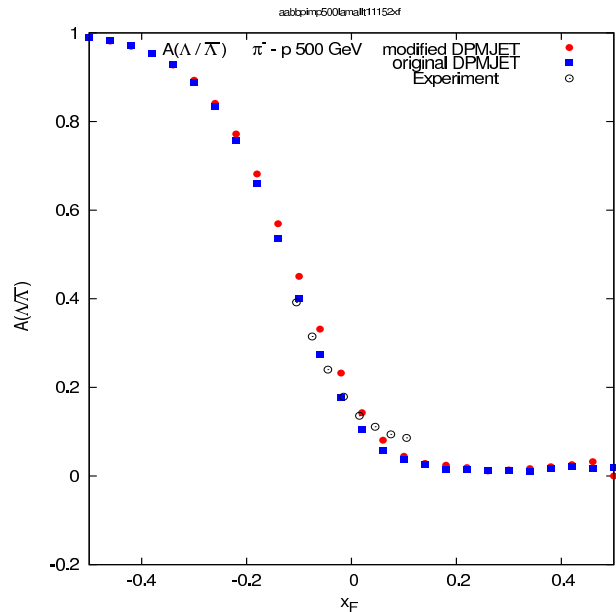


Figure 15: The  $A(\Lambda/\bar{\Lambda})$  asymmetry. Plotted are the original DPMJET-III, the modified DPMJET-III and the experimental data from the E791 Collaboration [9].

In Fig.15 we present the result for the  $A(\Lambda/\bar{\Lambda})$  asymmetry. We do not expect, that the mechanism according to Fig.14 changes the  $\Lambda$  or  $\bar{\Lambda}$  production in an essential way. Indeed we find in Fig.15 that the original DPMJET-III and the changed model agree perfectly with each other as well as with the data from the E791 Collaboration [9].

The  $A(\Xi/\bar{\Xi})$  and  $A(\Omega/\bar{\Omega})$  asymmetries are significantly modified by the mechanism according to Fig.14. We plot both asymmetries in Figs.16 and 17. Again the asymmetries according to the original and modified DPMJET-III are compared to the data from the E791 Collaboration [9]. With the original DPMJET-III the asymmetry  $A(\Xi/\bar{\Xi})$  is zero in the central region and the asymmetry  $A(\Omega/\bar{\Omega})$  is even negative in the central region. With the modified DPMJET-III both asymmetries become positive in the central region like the experimental data. For the chosen strangeness probability the  $\Omega$ -asymmetry is somewhat too strong while the  $\Xi$ -asymmetry is not sufficient.

Most significant seems the rise of of the  $\Xi$  asymmetry in the forward region. To investigate the influence of

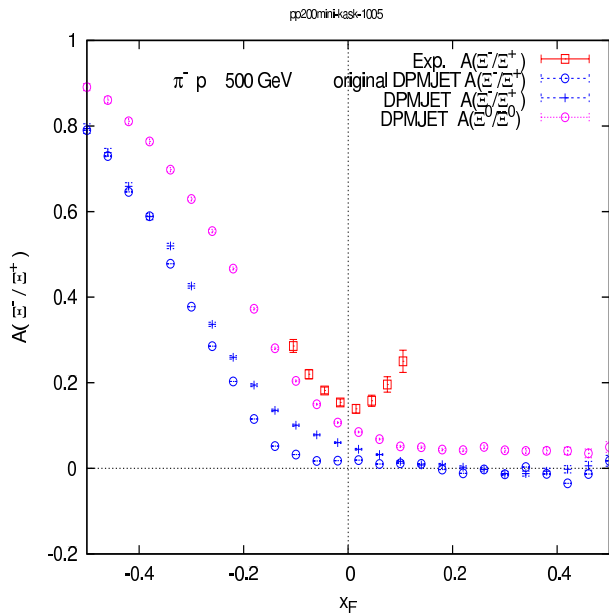


Figure 16: The  $A(\Xi/\bar{\Xi})$  asymmetry. Plotted are the original DPMJET-III, the modified DPMJET-III and the experimental data from the E791 Collaboration [9].

the meson isospin the net hyperon contributions are considered for various isospin combinations in Fig.18. The direct influence  $\pi^- \rightarrow \dots d \rightarrow dss$  seems not to reach the central region where baryons are sufficiently significant. Seen is a rank 2 effect  $\pi^- \rightarrow \dots \bar{u} \rightarrow \bar{u}d + \bar{d}\bar{s}\bar{s}$  which balancing contribution  $\pi^- \rightarrow \dots d \rightarrow \bar{d}d + \bar{d}\bar{s}\bar{s}$  is suppressed as  $m(\eta) \gg m(\pi^0)$ .

In conclusion the  $\pi^-$  isospin effect is not only too small to explain the effect but it actually contributes in the wrong direction.

The errorbars are significant. If the rise is confirmed by a second experiment again a new effect will have to be added. It could evidence the backward peak postulated in [39] caused by a tiny three chain forward-backward exchange contribution leaving a pion and possibly a  $ssd$  on the opposite side.

Rapidity distributions of  $p$ ,  $\bar{p}$ ,  $\Lambda$ ,  $\bar{\Lambda}$ ,  $\Xi$  and  $\bar{\Xi}$  were measured in proton-proton collisions at 158 GeV by the NA49 Collaboration [10]. Also in this experiment the  $\Xi/\bar{\Xi}$  ratio in the central region is found to be  $0.44 \pm 0.08$  that is smaller than 1. In the original DPMJET-III as well as in PYTHIA this ratio is found to be approximately equal to 1. The reasons for this are exactly the same as discussed above. In order to get a better agreement to the data, we have to modify DPMJET-III in the same way as described above, that is we have to include the mechanism according to Fig.14.

In Fig.19 we compare the results of the modified DPMJET-III (using  $B_{2Mesons} = 0.02$  und  $r_s = 30\%$ ) with the data from the NA49 Collaboration [10]. We find excellent agreements for  $p$ ,  $\bar{p}$ ,  $\Lambda$  and  $\bar{\Lambda}$  production and improved agreements for  $\Xi$  and  $\bar{\Xi}$  production.

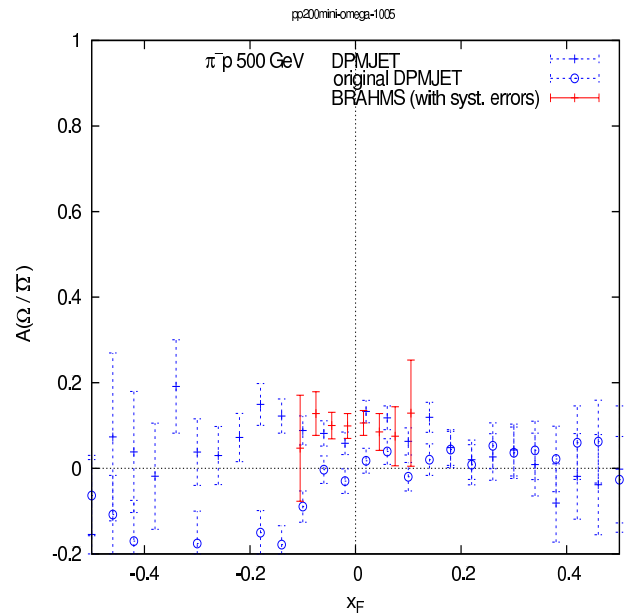


Figure 17: The  $A(\Omega/\bar{\Omega})$  asymmetry. Plotted are the original DPMJET-III, the modified DPMJET-III and the experimental data from the E791 Collaboration [9].

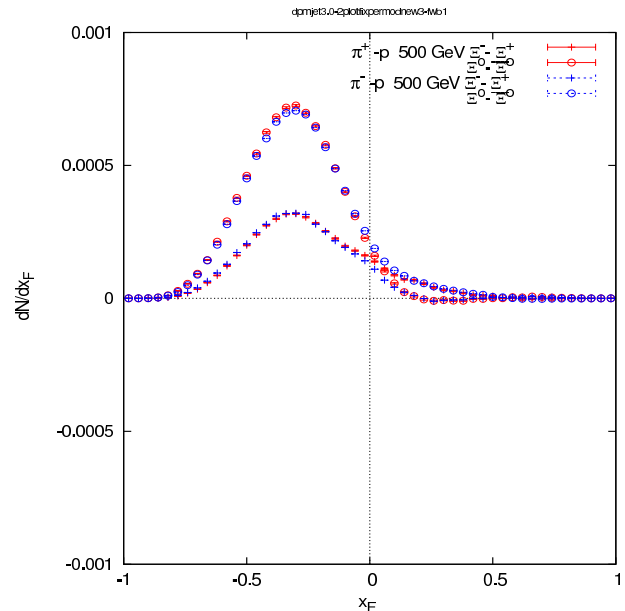


Figure 18: The net  $\Xi - \bar{\Xi}$  contribution for charged and neutral hyperons for  $\pi^+p$  and  $\pi^-p$  scattering.

## VI. SUMMARY

Experimental data are extremely useful to improve hadronic production models like DPMJET-III. Of particular importance in this respect are data on hadron production in hadron-hadron collisions and d-Au collisions measured at RHIC. In these collisions we found partly



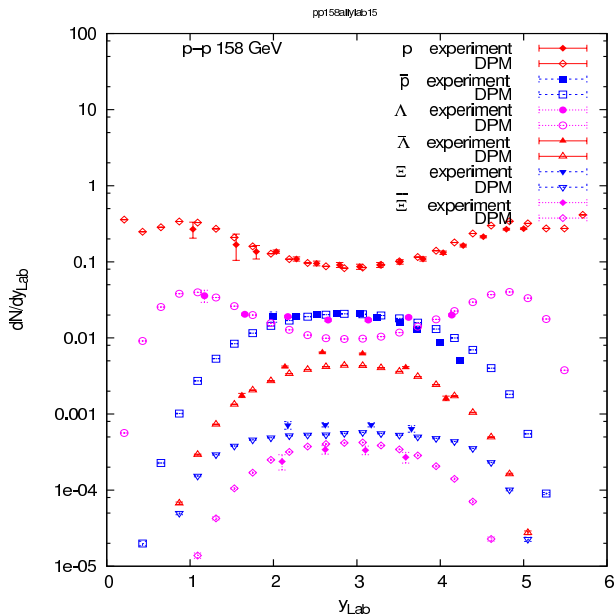


Figure 19: Rapidity distributions of produced  $p$ ,  $\bar{p}$ ,  $\Lambda$ ,  $\bar{\Lambda}$ ,  $\Xi$  and  $\bar{\Xi}$  in proton-proton collisions at 158 GeV. We compare the rapidity distributions according to the modified DPMJET-III with experimental data from the NA49 Collaboration [10].

already in previous papers[17, 18, 19] three important corrections to be applied to DPMJET-III:

- (i) Percolation and fusion of chains - the data from

RHIC allow to determine the amount of percolation to be implemented into DPMJET-III, see [17, 19].

- (ii) Collision scaling of large  $p_{\perp}$  hadron production in d-Au collisions, see [6].
- (iii) Replacing the Gaussian transverse momentum distribution contained in the JETSET-Pythia code [34, 35] by an exponential distribution in soft hadronic collisions, see [23].
- (iv) Implementation of new diagrams for an improved description of baryon stopping, see Figs. 2 and 4.
- (v) Adding the mechanism according to Fig.14 to the fragmentation of diquark chains

These corrections are somewhat technical, they do not involve the basic structure of the string model. In the considered not too dense region (hadron-hadron collisions and nuclear collisions involving light nuclei) the general features of the model can be considered as quite reliable.

In string models the baryon quantum number are carried by vortex lines which play a special role in the string structure. The understanding of baryon- and, in particular, the net-baryon-production is therefore of central importance.

In DPMJET-III, baryon stopping diagrams have to be included to get a consistent description of the considered RHIC data. With the new RHIC data, supporting anomalous baryon stopping, this is no longer a merely theoretical exercise. Good agreement with the critical experimental data was obtained.

- 
- [1] A. Capella, U. Sukhatme, C. I. Tan, and J. Tran Thanh Van, Phys. Rep. **236**, 227 (1994).
  - [2] R. Engel, Z. Phys. **C66**, 203 (1995).
  - [3] R. Engel and J. Ranft, Phys. Rev. **D54**, 4244 (1996).
  - [4] S. Roesler, R. Engel, and J. Ranft, Proceedings of ICRC 2001, Copernicus Ges. **1**, (2001).
  - [5] S. Roesler, R. Engel, and J. Ranft, [hep-ph/hep-ph/0012252], Proc. of Monte Carlo 2000, Lisboa, Oct.2000, Springer, p.1033, 1033 (2000).
  - [6] F.W.Bopp, J.Ranft, R.Engel and S.Roesler, [hep-ph/0403084 (unpublished).
  - [7] NA35 Collaboration, T. Alber *et al.*, Z. Phys. **C 64**, 195 (1994).
  - [8] NA35 Collaboration, T. Alber *et al.*, Eur. Z. Phys. **C2**, 643 (1998).
  - [9] E.M.Aitala *et al.* E791 Collaboration, Phys. Lett. B **469**, 9 (2000 [hep-ex/0009016]).
  - [10] T.Susa *et al.* NA49 Collaboration, Nucl. Phys. A **698**, 491c (2002).
  - [11] D. Kharzeev, Phys.Lett. **B 378**, 238 (1996).
  - [12] A. Capella and B. Kopeliovich, Phys. Lett. **B381**, 325 (1996).
  - [13] A. Capella, E. G. Ferreira, and C. A. Salgado, Phys. Lett. **B459**, 27 (1999).
  - [14] A. Capella and C. A. Salgado, Phys. Rev. C **60** (1999) 054906 [hep-ph/9903414].
  - [15] S. E. Vance and M. Gyulassy, Phys. Rev. Lett. **83**, 1735 (1999).
  - [16] J. A. Casado, Nucl.Phys. **A 651**, 93 (1999).
  - [17] J. Ranft, [hep-ph/0002137] (unpublished).
  - [18] J. Ranft, R. Engel, and S. Roesler, Proceedings of ICRC 2001, Copernicus Ges. , 435 (2001).
  - [19] J. Ranft, R. Engel, and S. Roesler, [hep-ph/0012112], Proc. of Monte Carlo 2000, Lisboa, Oct.2000, Springer, , 979 (2000).
  - [20] M. A. Braun, C. Pajares, and J. Ranft, Int. J. Mod. Phys. **A 14**, 2689 (1999).
  - [21] M. Braun and C. Pajares, Eur. Phys. J. **C16**, 359 (2000).
  - [22] J.Ranft, R.Engel and S.Roesler, Nucl. Phys. B (Proc. Suppl.) **122**, 292 (2003).
  - [23] F.W.Bopp, J.Ranft, R.Engel and S.Roesler, [hep-ph/410027] (to be published in proceedings).
  - [24] B.B.Back et al, PHOBOS Collaboration, Phys. Rev. C **70** (2004) 011901 [nucl-ex/0309013].
  - [25] P.Steinberg *et al.*, PHOBOS Collaboration, J. Phys. G;Nucl. Part. Phys.. **30**, S683 (2004)ls .
  - [26] F.Simon, STAR Collaboration, Acta Phys. Hung. A **27** (2006) 287 [nucl-ex/0412031] .
  - [27] I. G. Bearden *et al.*, BRAHMS Collaboration, Phys. Rev. Lett. **94**, 032301 (2005), [nucl-ex/0401025].
  - [28] I. G. Bearden *et al.*, BRAHMS Collaboration, Phys. Lett. B **607** (2005) 42, [nucl-ex/0409002].

- [29] G. C. Rossi and G. Veneziano, Nucl. Phys. **B123**, 507 (1977).
- [30] U. Sukhatme, K. Lassila and R. Orava, Phys.Rev. **D25**, 2075 (1982).
- [31] B. Z. Kopeliovich and B. G. Zakharov, Z. Phys. **C43**, 241 (1989).
- [32] J. Ranft and S. Ritter, Acta Phys. Pol. B **11**, 259 (1980).
- [33] S. Ritter, Comput. Phys. Commun. **31**, 393 (1984).
- [34] T. Sjöstrand, Comp. Phys. Comm. **82**, 74 (1994).
- [35] B. Andersson, G. Gustafson and T. Sjöstrand, Physica Scripta **32**, 574 (1985).
- [36] A Capella, E.G. Ferreiro, and C.A. Salgado, Nucl. Phys. **A 661**, 502 (1999).
- [37] F.W.Bopp and Yu.M.Shabelski, Phys. Atom. Nucl. **68**, 2093 (2005) [hep-ph/0406158]; F.W.Bopp and Yu.M.Shabelski, Eur. Phys. J. A **28**, 237 (2006) [hep-ph/0603193].
- [38] P. Aurenche and F. W. Bopp, Nucl. Phys. **B119**, (1977).
- [39] F. W. Bopp, [hep-ph/0002190] (unpublished).
- [40] Alper, B. *et al.*, Nucl. Phys. **B100**, 237 (1975).
- [41] M. Aguilar-Benitez *et al.*, Z. Phys. **C50**, 405 (1991).
- [42] G. H. Arakelian, A. Capella, A. B. Kaidalov and Y. M. Shabelski, Eur. Phys. J. C **26**, 81 (2002).
- [43] J.C.Dunlop for the STAR Collaboration, Nucl. Phys. A774:139-148, 2006 [nucl-ex/0510073].
- [44] J. Adams *et al.*, STAR Collaboration, Phys. Lett. B **637** (2006) 161 [nucl-ex/0601033].
- [45] A. Capella, Phys. Lett. B **542**, 65 (2002).
- [46] F.M.Liu *et al.*, Phys. Rev. D **67**, 034011 (2003).
- [47] This has the advantage, that we continue to use the standard PYTHIA and that we therefore will be able to replace PYTHIA with new versions.